J. Eng. Technol. Sci., Vol. 54, No. 1, 2022, 220112

Blasting Vibration Monitoring and a New Vibration Reduction Measure

Xi Yang, Yunpeng Zhang*& Jie Wang

North China University of Science and Technology, Hebei Mining Key Laboratory of Development and Safety Technology, Tangshan Hebei 063000, China
*E-mail: ncstzyp@163.com

Highlights:

- The peak particle velocity (PPV) and principal frequencies of different structures of single-story brick-concrete buildings are different. The PPV amplification factor does not change much when the principal frequency ratio is larger than 0.75.
- The measuring points of different heights have different sensitivities to blasting vibration waves of different principal frequencies.
- PPV can be reduced by waveform interference.

Abstract. Vibration waves generated by blasting can cause shock to buildings. Different responses occur in different parts of the building. Therefore, a single standard is inaccurate. At the same time, methods to reduce vibration are needed. In this paper, the variation of peak particle velocity (PPV) and principal frequency was analyzed. The energy variation of blast vibration waves was analyzed by wavelet packet decomposition. A numerical model was established to verify the new vibration reduction measure. The results showed that the PPV on the walls increases with their height. The PPV and principal frequency of different structures of single-story brick-concrete buildings are different. The amplification factor of PPV does not change much when the principal frequency ratio is larger than 0.75. Measuring points at different heights have different sensitivities to blasting vibration waves of different principal frequencies. Therefore, different structures will respond differently to the same blasting operation. The PPV can be reduced by waveform interference. However, the cycle of blasting vibration waves decreases with increasing distance. Therefore, it is necessary to determine a reasonable interval to reduce the PPV. This requires further research.

Keywords: *blasting vibration response; single-story brick-concrete buildings; PPV; principal frequency; vibration reduction measure.*

1 Introduction

Ore mining in open pits adversely affects the surrounding environment. Especially, vibration waves generated from blasting can cause shock to buildings around mines. If the vibration velocity exceeds a certain threshold, it will cause different degrees of damage to buildings around a mine [1-3]. This has a direct impact on the safety of people living around the mine [4-7]. Therefore, it is

Received October 8th, 2020, 1st Revision December 22nd, 2020, 2nd Revision July 29th, 2021, Accepted for publication September 29th, 2021.
 ISSN: 2337-5779, DOI: 10.5614/j.eng.technol.sci.2022.54.1.12

necessary to systematically study the vibration effect produced by blasting and take effective vibration reduction measures. Many villages and towns are situated in the vicinity of mines. The buildings are mostly single-story brick-concrete buildings. At present, relatively few studies have been conducted on this topic. It is necessary to conduct corresponding research.

Blasting vibration waves are affected by many factors [8-10]. Li, *et al.* [11] analyzed the PPV and stress on a tunnel surface, after which they assessed the tunnel's safety. Xia, *et al.* [12] found that the damage degree to rock on the tunnel surface increased with the increase of PPV. Kahriman [13] predicted the PPV in a limestone quarry and eliminated environmental problems around the quarry. Abiodun Ismail Lawal proposed an artificial neural network-based mathematical model for the prediction of blast-induced ground vibrations [14-18]. Singh, *et al.* [19,20] analyzed blast signatures and proposed an effective charge weight for the prediction of ground vibrations. Smerzini, *et al.* [21] proposed a method for describing ground vibrations generated by P, S or R seismic waves. Xu Jingui [22] found that blasting vibrations decreased with the increase of horizontal distance. The blasting vibration velocity at the top of the slope was obviously higher than that in the other positions. Qiu Xianyang [23] revealed the time-frequency characteristics of vibration signals. The most important ones among these factors are PPV and frequency. Blast vibration standards have been proposed to protect buildings and limit blasting vibration. Frequency and PPV are considered in these standards. The United States Bureau of Mines (USBM) published RI 8507 [24] and recommended blasting level criteria that set a peak particle limit based on the predominant frequency of the seismic wave. Other countries have proposed corresponding standards [25,26]. These standards are similar; all of them limit the PPV in different frequency ranges. As an example, one of them is shown in Table 1.

Table 1 Permissible peak particle velocity (PPV) in mm/s at the foundation level of structures in mining areas (DGMS circular 7 of 1997).

	Dominant excitation frequency/ Hz		
	<8Hz	**8-25Hz**	**>25Hz**
(A) Buildings/structures not belonging to the mine owner			
1. Domestic houses/structures (Mud/ Kuchcha, brick and cement)	5	10	15
2. Industrial buildings	10	20	25
3. Objects of historical importance and sensitive structures	2	5	10
(B) Buildings belonging to the mine owner with limited life span			
1. Domestic houses/structures	10	15	25
2. Industrial buildings	15	25	50

The PPV and frequency in these standards are definite values. However, the PPV and frequency of different structures of the buildings respond differently to the same blasting. At the same time, the PPV and frequency at different heights are also different. Building types are mentioned in these standards. However, structures of buildings are not mentioned. The damage to structures of buildings by PPV and frequency is different; people also respond to them differently. This needs to be further clarified. Since blasting vibration can damage houses, it must be investigated how we can reduce its impact. Various methods and techniques have been developed to reduce blasting vibrations [27,28]. The water jet technique has been frequently applied in many different fields [29-32]. It was developed by Jung-Gyu Kim [33] to block the propagation of vibrations from tunnel blasting. At the same time, many different vibration control methods have been developed [34,35]. These methods can be classified into four major categories: passive control [36,37], semi-active control [38,39], active control [40], and hybrid control [41]. However, these methods require additional facilities, or the structure of the building must be changed. This increases the investment capital required. Blasting vibration waves respond differently to different structures of the building. Different vibration control methods should be adopted for different structures of a building, or the vibration of the building should be reduced by reducing the blasting vibration waves. However, the effect of blasting excavation cannot be reduced. Therefore, new vibration reduction measures should be considered.

In this paper, blast vibration monitoring was conducted for different structures of single-story brick-concrete buildings. The variation of PPV and principal frequency was analyzed. The energy variation of blast vibration waves was analyzed by wavelet packet decomposition. A numerical model was established to verify the new vibration reduction measure that can be used to protect buildings near mines.

2 Experimental Site and Experimental Details

Single-story brick-concrete buildings are situated near an opencast mine in the east of Hebei Province, China, as shown in Figure 1. The mine produces millions of tons of iron ore every year. Ground vibrations from blasting have been a continuous problem for the mine and the surrounding buildings. Hole-by-hole detonation technology has been adopted in the mine. The explosive weight in each hole is between 100 kg and 480 kg. Different explosive weights are adopted in different locations according to work requirements.

The monitoring equipment was a TC-4850 blasting vibration intelligent monitor produced by the Chinese Academy of Sciences. It can accurately monitor the

waveform, the principal frequency and the PPV of the blasting vibration waves. The monitoring points are shown in Figure 2.

Figure 1 Monitoring location.

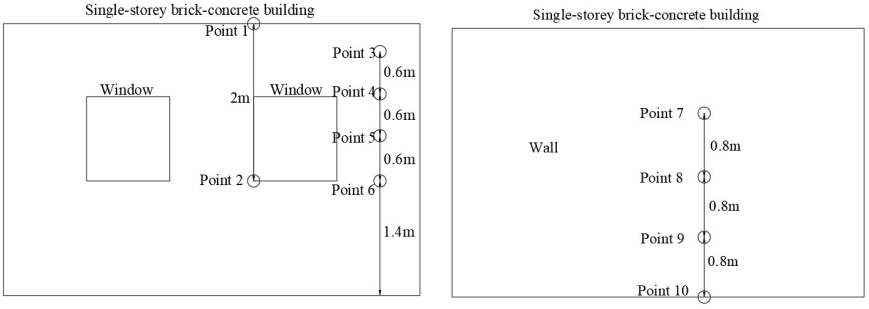

(a) Monitoring points on external wall (b) Monitoring points on inner wall

Figure 2 Monitoring points of single-story brick-concrete building.

3 Vibration Monitoring on the Structures

In total, six tests were conducted. The principal frequency and PPV of the blasting vibration waves are shown in Table 2. The X direction is perpendicular to the Y and Z directions. The Y direction points toward the blasting site. The Z direction is perpendicular to the ground.

The PPV of monitoring points 3, 4, 5, 6 in the X direction are presented in Figure 3. The PPV of monitoring points 3, 4, 5, 6 in the Y direction are shown in Figure 4. The PPV of monitoring points 3, 4, 5, 6 in the Z direction are shown in Figure 5. The PPV near the corner of a wall increases with height. However, this is not obvious in the Z direction.

Table 2 PPV and principal frequency.

Number	Points	X		Y		Z	
		PPV /mm·s^{-1}	Principle frequency/ Hz	PPV /mm·s^{-1}	Principle frequency /Hz	PPV /mm·s^{-1}	Principle frequency /Hz
1	1	1.059	11.6822	4.693	9.8039	1.65	12.4378
	2	0.97	7.4850	4.35	9.3633	1.401	13.1579
	3	1.119	8.4459	4.598	9.8425	1.373	11.7925
	4	1.035	8.3333	4.296	9.7276	1.423	12.0773
	5	0.857	7.6340	4.123	9.7320	1.359	11.7650
	6	0.927	7.5988	3.466	9.5057	1.373	11.9048
	7	0.311	5.3050	0.479	10.7820	0.333	6.8850
	8	0.295	6.6450	0.419	7.4630	0.293	9.5240
	9	0.247	5.8060	0.382	7.1170	0.312	6.6010
	10	0.344	5.4790	0.387	7.3390	0.436	6.7230
2	1	3.249	8.3612	6.899	12.3762	3.477	11.6279
	2	2.395	8.3893	4.809	11.3122	2.889	10.9170
	3	3.488	7.9872	6.325	12.3762	3.149	12.0773
	4	3.116	8.1169	5.727	12.1359	3.396	11.4679
	5	2.571	8.3860	5.434	11.7650	3.206	11.5940
	6	2.373	8.5074	4.192	11.1607	3.03	11.6279
	7	3.012	9.8770	5.737	11.9760	3.458	14.9250
	8	2.518	9.5690	4.762	11.4940	3.263	14.9810
	9	2.129	6.7230	3.191	16.6670	2.151	28.7170
	10	3.682	13.6050	6.173	30.7690	5.214	20.2020
3	1	0.824	14.1243	1.185	14.1243	0.685	15.5280
	2	0.492	9.1575	0.964	10.4603	0.6	12.5000
	3	0.782	13.9665	1.132	14.3678	0.621	15.5280
	4	0.666	13.8889	1.05	13.9665	0.602	11.1111
	5	0.518	9.7090	1.014	10.4710	0.55	10.9590
	6	0.507	8.6505	0.867	10.8695	0.58	11.2613
	7	0.697	14.2350	1.016	10.4440	0.655	12.2700
	8	0.59	12.9870	0.836	10.5540	0.575	13.0290
	9	0.472	14.5450	0.813	10.3630	0.502	12.1950
	10	0.73	14.7600	0.607	8.6960	0.993	17.7780
4	1	1.389	10.2881	1.314	17.6056	0.723	18.3824
	2	0.844	8.8339	1.011	24.0385	1.3	13.2979
	3	1.395	10.9649	1.109	17.4825	0.688	18.2482
	4	1.189	10.2881	1.062	17.9856	0.679	17.7305
	5	0.91	9.9260	1.058	16.4610	0.571	17.0990
	6	0.853	9.1575	0.89	16.0256	0.544	18.2482
	7	0.836	8.8500	1.115	17.0210	0.891	12.9030
	8	0.748	9.0910	0.894	15.6250	0.824	13.6050
	9	0.665	8.9690	0.789	14.7060	0.846	13.5590
	10	1.363	35.0880	2.142	28.1690	1.724	17.4670
5	1	2.095	12.1359	6.054	9.8039	2.259	10.5932
	2	1.538	8.0645	5.161	9.6525	2.164	9.0909
	3	2.574	10.5932	5.847	9.8039	1.917	10.0000
	4	2.355	9.6154	5.274	9.8039	1.948	9.2937
	5	1.703	8.2990	5.17	9.5690	1.971	10.2040
	6	1.423	10.7759	4.731	10.5485	1.885	17.4825
	7	1.833	9.2810	5.223	9.5690	1.761	9.8520
	8	1.496	8.0970	4.592	9.2810	1.518	13.6050
	9	1.395	7.8740	4.052	10.1320	1.7	12.5000
	10	2.34	9.6620	4.23	10.5540	2.291	18.3490

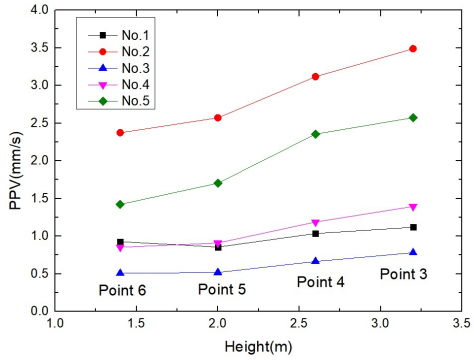

Figure 3 PPV of monitoring points 3, 4, 5, 6 in the X direction.

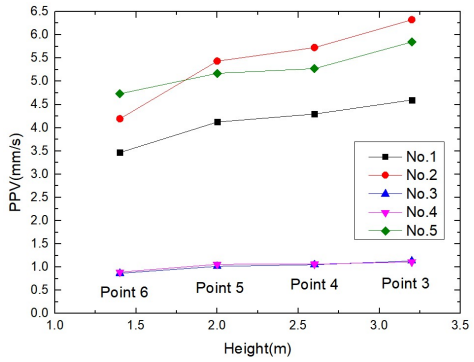

Figure 4 PPV of monitoring points 3, 4, 5, 6 in the Y direction.

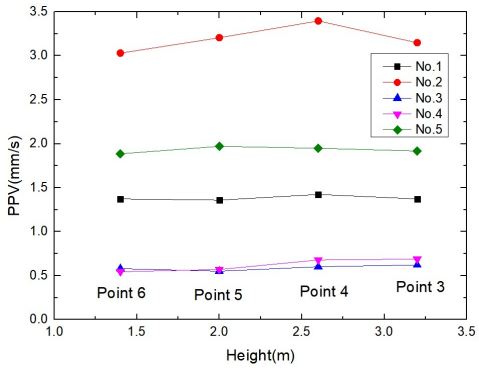

Figure 5 PPV of monitoring points 3, 4, 5, 6 in the Z direction.

The PPV of monitoring points 7, 8, 9, 10 in the X, Y, Z directions are presented in Figures 6, 7, and 8 respectively. The PPV decreases first and then increases with height. The PPV on the ground is larger than the PPV on the walls near it, while the PPV on the walls increases with height.

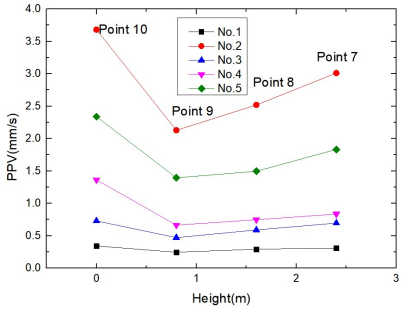

Figure 6 PPV of monitoring points 7, 8, 9, 10 in the X direction.

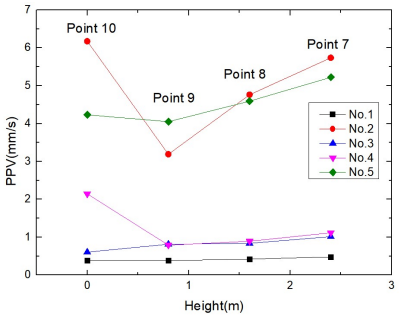

Figure 7 PPV of monitoring points 7, 8, 9, 10 in the Y direction.

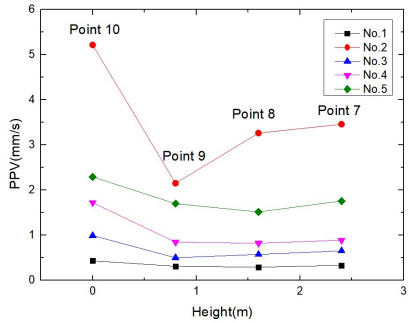

Figure 8 PPV of monitoring points 7, 8, 9, 10 in the Z direction.

The PPV on a high wall is larger than the PPV on the ground. As shown in Table 3, the PPV on the roof is larger than the PPV on the ground. The PPV on the roof is also larger than the PPV on the windows. This is a PPV amplification phenomenon related to height. The PPV on a window is larger than on a corner when the height is the same. Because blasting vibration waves cause different responses in different structures, the PPV and principal frequency of different structures of single-story brick-concrete buildings are different. The vibration resistance of different structures is also different. Therefore, a single standard is inaccurate.

Table 3 PPV on different structures.

Number	Point	X	Y	Z
		PPV/mm·s^{-1}	PPV/mm·s^{-1}	PPV/mm·s^{-1}
1	1 (Roof)	1.059	4.693	1.65
	2 (Window)	0.97	4.35	1.401
	6 (Corner)	0.927	3.466	1.373
	10 (Ground)	0.344	0.387	0.436
2	1 (Roof)	3.249	6.899	3.477
	2 (Window)	2.395	4.809	2.889
	6 (Corner)	2.373	4.192	3.03
	10 (Ground)	3.682	6.173	5.214
3	1 (Roof)	0.824	1.185	0.685
	2 (Window)	0.492	0.964	0.6
	6 (Corner)	0.507	0.867	0.58
	10 (Ground)	0.73	0.607	0.993
4	1 (Roof)	1.389	1.314	0.723
	2 (Window)	0.844	1.011	1.3
	6 (Corner)	0.853	0.89	0.544
	10 (Ground)	1.363	2.142	1.724
5	1 (Roof)	2.095	6.054	2.259
	2 (Window)	1.538	5.161	2.164
	6 (Corner)	1.423	4.731	1.885
	10 (Ground)	2.34	4.23	2.291

Principal frequency ratio λ is shown in Eq. (1).

$$\lambda = \frac{f_w}{f} \tag{1}$$

where f_w is the vibration principal frequency of the ground, f is the vibration principal frequency of different structures.

The amplification factor is shown in Eq. (2).

$$\beta = \frac{\ddot{x}_{\max}}{\left|\ddot{x}_g\right|_{\max}} = \frac{v_h}{v_h^g} \tag{2}$$

where β is the amplification factor, v_h is the PPV at different points, v_h^g is the PPV on the ground.

The amplification factor and principal frequency ratio in the X, Y, Z directions are shown in Figures 9, 10, and 11 respectively. The amplification factor increases rapidly when the principal frequency ratio is less than 0.75. The amplification factor does not change much when the principal frequency ratio is larger than 0.75. The principal frequency may be close to the natural frequency of different structures.

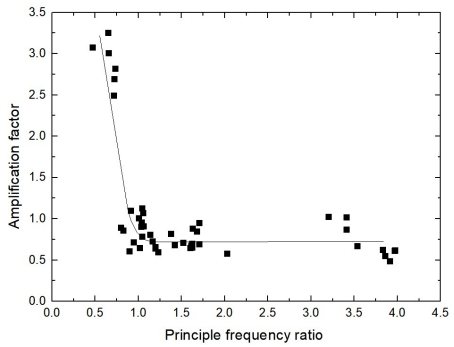

Figure 9 Amplification factor and principal frequency ratio in the X direction.

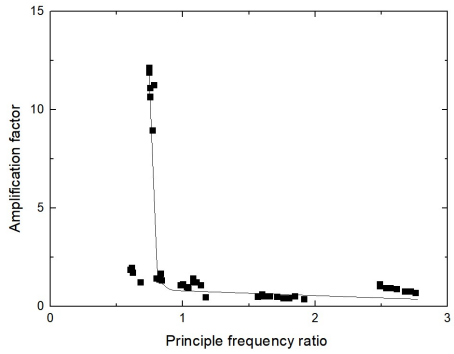

Figure 10 Amplification factor and principal frequency ratio in the Y direction.

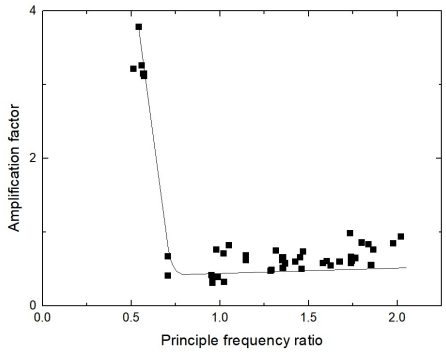

Figure 11 Amplification factor and principal frequency ratio in the Z direction.

As shown in Figure 12, the energy ratio of the measuring points was obtained by wavelet packet decomposition. The size of each frequency band was 7.81 Hz (frequency band 1 was from 0 Hz to 7.81 Hz, frequency band 2 was from 7.81 Hz to 15.62Hz). In the low frequency band (frequency bands 2, 3, 4), the energy ratio at a low point was large. In the high frequency bands (frequency bands 7 and 8), the energy ratio at a high point was large. This shows that the measuring points at different heights have different sensitivities to blasting vibration waves of different principal frequencies. Therefore, different structures respond differently to the same blasting operation.

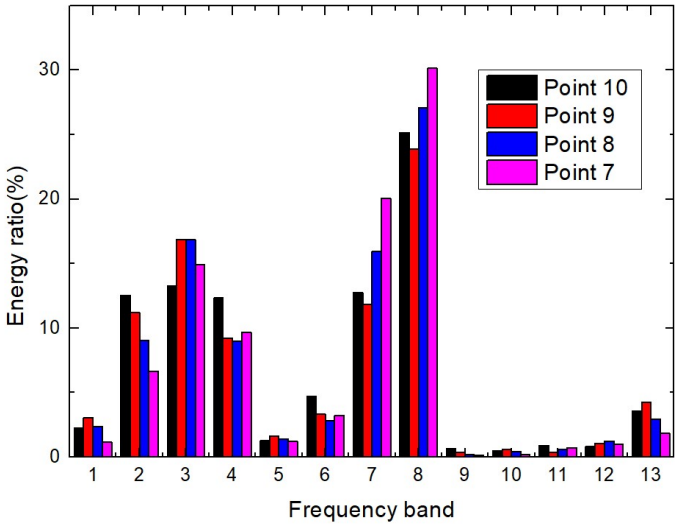

Figure 12 Energy ratio of the measuring points.

4 Vibration Reduction Measures

Previous vibration reduction methods require additional facilities, or the structure of the building must be changed. This increases the investment capital required. Waveform interference does not require more investment capital. As shown in Figure 13, the two waveforms will be reduced after superposition. How do we implement this method? First, Ls-dyna is used to establish a model, as shown in Figure 14. The model width is 100 m. The height is 24 m. Second, MAT_HIGH_EXPLOSIVE_ BURN material is used for the explosive. The JWL equation for describing explosions is shown as Equation 3. The parameters of the explosive are shown in Table 4. MAT_PLASTIC_KINEMATIC material is used for rock. The parameters of rock are shown in Table 5.

$$P = A(1-\frac{\omega}{R_1 V})e^{-R_1 V} + B(1-\frac{\omega}{R_2 V})e^{-R_2 V} + \frac{\omega E_0}{V} \tag{3}$$

where P is detonation pressure, V is the relative volume, E_0 the initial specific internal energy, and A, B, R_1, R_2 and ω are independent constants describing the JWL equation.

Thirdly, the meshing is shown in Figure 15. The bottom of the model is a non-reflective boundary. Lastly, the simulation time is 50,000 μs.

The velocity time history at point A in the model of one 500-kg explosive package is shown in Figure 16. The PPV of point A is 100cm/s.

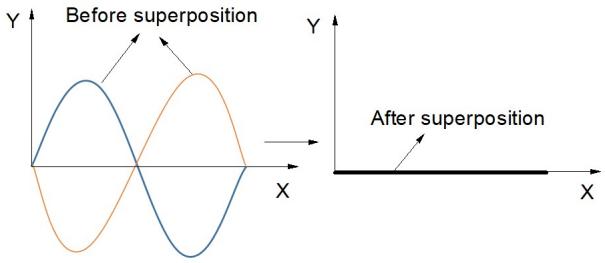

Figure 13 Waveform interference.

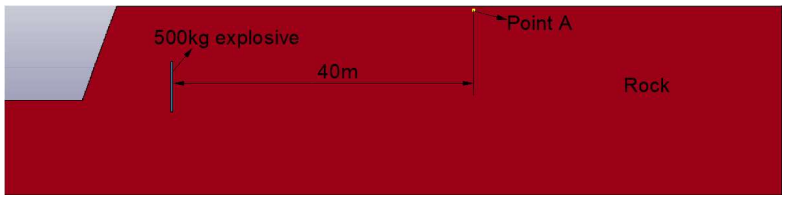

Figure 14 The model of one 500-kg explosive package.

Table 4 Parameters of explosive.

Density (g/cm^3)	Detonation speed (m/s)	A (GPa)	B (GPa)	R_1	R_2	ω
1.0	5000	214	0.18	4.2	0.8	0.15

Table 5 Rock parameters.

Density (g/cm^3)	Young's modulus (GPa)	Poisson's ratio	Yield stress (MPa)	Tangent modulus (GPa)	Hardening parameter
2.54	57	0.27	106	5.5	0.5

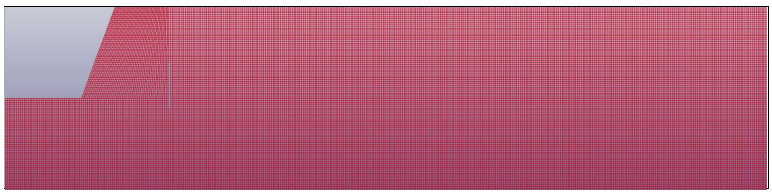

Figure 15 Meshing.

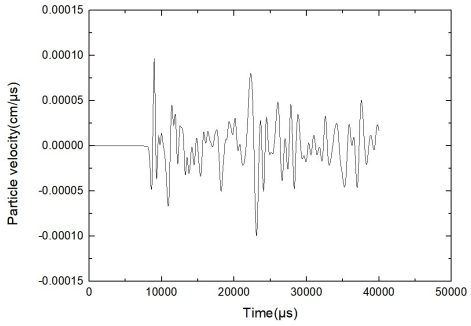

Figure 16 Velocity time history at point A in the model of one 500-kg explosive package.

Firstly, Ls-dyna is used to establish another model, as shown in Figure 17. The model width is 100 m. The height is 24 m. The 500-kg explosive is divided into two 250-kg explosives. The two 250-kg explosive packages detonate at the same time. Two explosives are separated by air. Secondly, the Gruneisen equation for describing air under high pressure is shown in Equation 4. The air parameters are shown in Table 6. The material parameters of rock and explosive are the same as in the previous model. Thirdly, the meshing is shown in Figure 18. The bottom of the model is a non-reflective boundary. Lastly, the simulation time is 50,000 μs.

The velocity time history at point B in the model with two 250-kg explosive packages is shown in Figure 19. The PPV at point B is 90 cm/s. It is less than that at point A, because the waveforms of the two 250-kg explosive packages interfere with each other, as can be seen from Figure 21. The waveform interference is affected by the initial phase of the blasting vibration wave if the initial phases of the two blasting vibration waves are opposite, as shown in Figure 21. The two explosive packages should be detonated at the same time. If the initial phases of the two blasting vibration waves are the same, the initiation detonation time of the two explosive packages should be half a cycle apart. However, the cycle of blasting vibration waves decreases with increasing distance. The PPV can be reduced by taking different intervals between two explosive packages according to the cycle of different locations, so the cycle is changed in a blasting vibration wave. Therefore, it is necessary to determine a reasonable interval to reduce the PPV. This requires further research.

$$P = \frac{\rho_0 C^2 \mu[1+(1-\frac{\gamma_0}{2})\mu - \frac{a}{2}\mu^2]}{[1-(S_1-1)\mu - S_2\frac{\mu^2}{\mu+1} - S_3\frac{\mu^3}{(\mu+1)^2}]^2} + (\gamma_0 + a\mu)E_0 \tag{4}$$

where ρ_0 is initial density, γ_0 is the Gruneisen parameter, E_0 is initial internal energy, C is the curve intercept, S_1, S_2, S_3 are curve slope coefficients, μ is the dynamic viscosity coefficient, a is a first-order volume correction of γ_0 and μ.

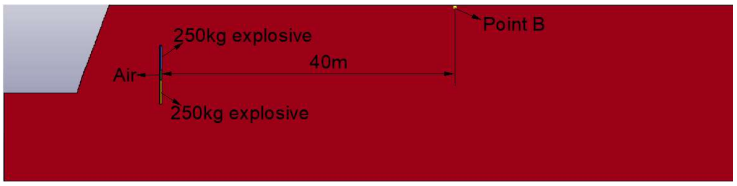

Figure 17 The model of two 250kg explosive packages.

Table 6 Air parameters.

Density (g/cm^3)	C	S_1	S_2	S_3	μ	γ_0	E_0
1.239×10^{-3}	0.344	0	0	0	8.9×10^{-4}	1.4	0

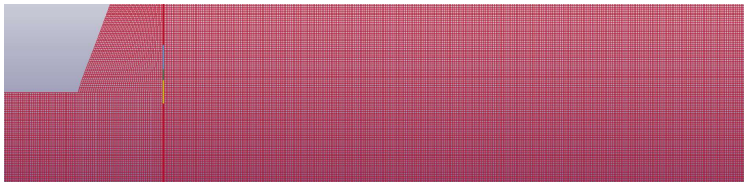

Figure 18 Meshing.

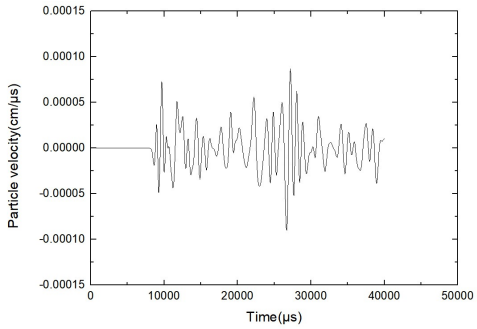

Figure 19 Velocity time history at point B in the model with two 250-kg explosive packages.

Figure 20 Points C and D.

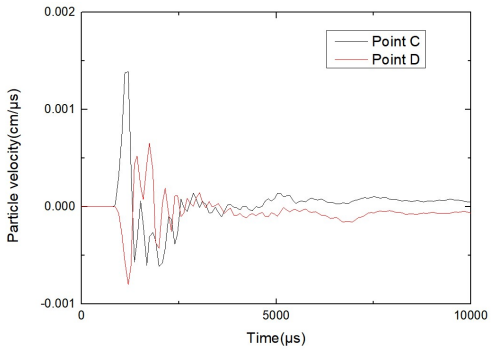

Figure 21 The waveform interference of the model with two 250-kg explosive packages.

5 Conclusion

The PPV on a wall increases with its height. The PPV and principal frequencies of different structures of single-story brick-concrete buildings are different. The vibration resistance of different structures is also different. Therefore, a single standard is inaccurate.

The amplification factor of the PPV does not change much when the principal frequency ratio is larger than 0.75. This is maybe because the principal frequency is close to the natural frequency of different structures. Measuring points at different heights have different sensitivities to blasting vibration waves of different principal frequencies. Therefore, different structures will respond differently to the same blasting operation. It is necessary to propose a PPV limit standard for different structures of single-story brick-concrete buildings or other buildings. This can better balance mine production and building safety. This requires further research.

PPV can be reduced by waveform interference. Waveform interference is affected by the initial phase of the blasting vibration wave. If the initial phases of the two blasting vibration waves are opposite, the two explosive packages should be detonated at the same time. If the initial phases of the two blasting vibration waves are the same, the initiation detonation time of the two explosive packages should be half a cycle apart. However, the cycle of blasting vibration waves decreases with increasing distance. It also changes in the blasting vibration wave. Therefore, it is necessary to determine a reasonable interval to reduce PPV. This requires further research.

Acknowledgement

This research was mainly supported by the National Natural Science Foundation of China (51774137) and National Key Technologies Research & Development Program (2017YFC0804609).

References

[1] Nateghi, R., Kiany, M. & Gholipouri, M., *Control Negative Effects of Blasting Waves on Concrete of the Structures by Analyzing of Parameters of Ground Vibration*, Tunneling and Underground Space Technology, **24**, pp. 608-616, 2009.

[2] Kahriman, A., *Analysis of Ground Vibrations Caused by Bench Blasting at Can Open-Pit Lignite Mine in Turkey*, International Journal of Geosciences Environmental Geology, **41**(6), pp. 653-661, 2002.

[3] Karadogan, A., *The Investigation of Establishing the National Structure Damage Criteria for the Ground Vibration Induced by Blasting*, Doctorate thesis. Istanbul, Turkey: Istanbul University, 2008.

[4] Ak, H., Iphar, M., Yavuz, M. & Konuk, A., *Evaluation of Ground Vibration Effect of Blasting Operations in a Magnesite Mine*, Soil Dynamics and Earthquake Engineering, **29**(4), pp. 669-676,2009.

[5] Elevli, B. & Arpaz, E., *Evaluation of Parameters Affected on the Blast Induced Ground Vibration by Using Relation Diagram Method*, Acta Montanistica Slovaca, **15**(4), pp. 261-268, 2010.

[6] Nateghi, R., *Prediction of Ground Vibration Level Induced by Blasting at Different Rock Units*, International Journal of Rock Mechanics and Mining Sciences, **48**(4), pp. 899-908, 2011.

[7] Angel, U., Alberto, P., Olga, V., Bruna, G., Faycal, B. & Cesar, A., *ESPRES: A web Application for Interactive Analysis of Multiple Pressures in Aquatic Ecosystems*, Science of the Total Environment, **744**, 140792, 2020.

[8] Lu, Y., *Underground Blast Induced Ground Shock and Its Modelling Using Artificial Neural Network*, Comp. Geotech., **32**, pp. 164-178, 2005.

[9] Guan, X., Wang, X. & Zhu, Z., *Ground Vibration Test and Dynamic Response of Horseshoe-shaped Pipeline During Tunnel Blasting Excavation in Pebbly Sandy Soil*, Geotechnical and Geological Engineering, **38**(1), pp. 3725-3736, 2020.

[10] A K W, B X Q & B Z L, *Experimental and Numerical Investigations on Predictor Equations for Determining Parameters of Blasting-Vibration on Underground Gas Pipe Networks*, Process Safety and Environmental Protection, **133**, pp. 315-331, 2020.

[11] Li, JC., Li, HB., Ma, GW. & Zhou, YX., *Assessment of Underground Tunnel Stability to Adjacent Tunnel Explosion*, Tunn. Undergr. Space Technol., **35**, pp. 227-234, 2013.

[12] Xia, X., Li, H.B., Li, J.C., Liu, B. & Yu, C., *A Case Study on Rock Damage Prediction and Control Method for Underground Tunnels Subjected to Adjacent Excavation Blasting*, Tunn. Undergr. Space Technol., **35**, pp. 1-7, 2013.

[13] Kahriman, A., *Analysis of Parameters of Ground Vibration Produced from Bench Blasting at a Limestone Quarry*, Soil. Dyn. Earthquake Eng., **24**, pp. 887-892, 2004.

[14] Lawal, A.I., Kwon, S., & Kim, G.Y., *Prediction of the Blast-induced Ground Vibration in Tunnel Blasting Using ANN, Moth-flame Optimized ANN, and Gene Expression Programming*, Acta Geophysica, **69**, pp. 161-174, 2021.

[15] Lawal, A.I., & Kwon, S., *Application of Artificial Intelligence to Rock Mechanics: An Overview*, Journal of Rock Mechanics and Geotechnical Engineering, **13**, pp. 248-266, 2021.

[16] Lawal, A.I., & Idris, N.A., *An Artificial Neural Network-based Mathematical Model for the Prediction of Blast-induced Ground Vibrations*, International Journal of Environmental Studies, **77**, pp. 318-334, 2020.

[17] Lawal, A.I., *An Artificial Neural Network-based Mathematical Model for the Prediction of Blast-induced Ground Vibration in Granite Quarries in Ibadan, Oyo State, Nigeria*, Scientific African, **8**, e00413, 2020.

[18] Lawal, A.I., *A New Modification to the Kuz-Ram Model using the Fragment Size Predicted by Image Analysis*, International Journal of Rock Mechanics and Mining Sciences, **138**, 104595, 2021.
[19] Singh, P.K., Sirveiya, A.K., Roy, M.P., Prasad, A. & Mohapatra, T., *A New Approach in Blast Vibration Analysis and Prediction at Iron Ore Mines*, Min. Technol. (Trans Inst Min Metall A), **114**(4), pp. A209-218, 2005.
[20] Singh, P.K., Sirveiya, A.K., Babu, K.N., Roy, M.P. & Singh, C.V., *Evolution of Effective Charge Weight per delay for Prediction of Ground Vibrations Generated from Blasting in a Limestone Mine*, Int. J. Min. Reclam. Environ., **20** (1), pp. 4-19, 2006.
[21] Smerzini, J.C., Aviles, R., Paolucci, F.J. & Sesma, S., *Effect of Underground Cavities on Surface Ground Motion under SH Wave Propagation*, Earthq. Eng. Struct. Dyn., **398**, pp. 1441-1460, 2009.
[22] Xu, J., Pu, C., He, G., Xiao, D. & Feng, Y., *Experimental Study on Propagation of Side Slope of Blasting Vibration of Mountain-adjacent Tunnel*, Nonferrous Metals (Mine Section), **70**(3), pp. 51-58, 112, 2018.
[23] Qiu, X., Shi, X., Zhou, J., Huang, D. & Chen, X., *On Vibration Reduction Effect of Short Millisecond Blasting by High-precision Detonator based on HHT Energy Spectrum*, Explosion and Shock Waves, **37**(1), pp. 107-113, 2017.
[24] Siskind, D.E., Stagg, M.S., Kopp, J.W. & Dowding, C.H., *Structure Response and Damage Produced by Ground Vibration from Surface Mine Blasting*, US Bur Mines Rep Invest, **74**, 8507, 1980.
[25] German Institute of Standards, *Vibration of Building-effects on Structures*, DIN 4150, **3**, pp. 1-5, 1986.
[26] DGMS (Tech) S&T Circular No. 7, *Damage of the Structures due to Blast induced Ground Vibration in the Mining Areas*, 1997.
[27] Prakash, A.J., Palroy, P. & Misra, D.D., *Analysis of Blast Vibration Characteristics Across a Trench and a Pre-split Plane*, Fragblast, **8**(1), pp. 51-60, 2004.
[28] Erarslan, K., Uysal, Ö., Arpaz, E. & Cebi, M.A., *Barrier Holes and Trench Application to Reduce Blast Induced Vibration in Seyitomer coal mine*, Environ. Geol., **54**(6), pp. 1325-1331, 2008.
[29] Alberdi, A., Suárez, A., Artaza, T., Escobar-Palafox, G.A. & Ridgway, K., *Composite Cutting with Abrasive Water Jet*, Procedia Eng., **63**, pp. 421-429, 2013.
[30] Guha, A., Barron, R.M. & Balachandar, R., *An Experimental and Numerical Study of Water Jet Cleaning Process*, J. Mater Process Technol., **211**(4), pp. 610-618, 2011.
[31] Momber, AW., Kovacevic, R. & Mohan, R., *Fracture Range Detection in the Hydroabrasive Erosion of Concrete*, Wear, **253**, pp. 156-1164, 2002.
[32] Schumacher, B., Charton, J.P., Nordmann, T., Vieth, M., Enderle, M. & Neuhaus, H., *Endoscopic Submucosal Dissection of Early Gastric*

Neoplasia with a Water Jetassisted Knife: a Western, Single-center Experience, Gastrointest Endosc, **75**(6), pp. 1166-1174, 2012.

[33] Jung-Gyu, K. & Jae-Joon, S., *Abrasive Water Jet Cutting Methods for Reducing Blast-induced Ground Vibration in Tunnel Excavation*, International Journal of Rock Mechanics & Mining Sciences, **75**, pp. 147-158, 2015.

[34] Zhang, C., Li, J. & Bi, K., *Preface: Recent Advances on Structural Control, Health Monitoring and Applications in Bridge Engineering*, Int. J. Struct. Stab. Dyn., **18**(8), 1802001, 2018.

[35] Song, G., Cai, S. & Li, H.N., *Energy Dissipation and Vibration Control: Modeling, Algorithm, and Devices*, Appl. Sci., **801**(8), 7, 2017.

[36] Lackner, M.A. & Rotea, M.A., *Passive Structural Control of Offshore Wind Turbines*, Wind Energy, **14**(3), pp. 373-388, 2011.

[37] Wang, W., Hua, X., Wang, X., Chen, Z. & Song, G., *Numerical Modeling and Experimental Study on a Novel Pounding Tuned Mass Damper*, J. Vib. Control., **24**(17), pp. 4023-4036, 2018.

[38] Behrooz, M., Wang, X. & Gordaninejad, F., *Modeling of a New Semi-active/passive Magnetorheological Elastomer Isolator*, Smart Mater. Struct., **23**(4), 045013, 2014.

[39] Shirazi, F.A., Mohammadpour, J., Grigoriadis, K.M. & Song, G., *Identification and Control of an MR Damper with Stiction Effect and its Application in Structural Vibration Mitigation*, IEEE T. Contr. Syst. T., **20**(5), pp. 1285-1301, 2012.

[40] Zhang, C. & Hao, W., *Robustness of the Active Rotary Inertia Driver System for Structural Swing Vibration Control Subjected to Multi-Type Hazard Excitations*, Appl. Sci.-Basel, **9**(20), pp. 1-16, 2019.

[41] Demetriou, D. & Nikitas, N., *A Novel Hybrid Semi-active Mass Damper Configuration for Structural Applications*, Appl. Sci., **6**(12), 397, 2016.